Model-independent interpretation of the dynamic hyperfine effect in muonic atoms with an application to ^{192}Os†

L. K. Wagner*
The Florida State University, Tallahassee, Florida 32306
and University of California, Los Alamos Scientific Laboratory, Los Alamos, New Mexico 87545

E. B. Shera
University of California, Los Alamos Scientific Laboratory, Los Alamos, New Mexico 87545

G. A. Rinker
University of California, Los Alamos Scientific Laboratory, Los Alamos, New Mexico 87545
and Institut für Kernphysik Kernforschungsanlage Jülich, D-5170 Jülich, West Germany

R. K. Sheline
The Florida State University, Tallahassee, Florida 32306
(Received 15 March 1977)

The Ford-Wills-Barrett model-independent interpretation of muonic-atom transition energies is generalized to the dynamic hyperfine effect. Parameters necessary for the analysis of the most important case (quadrupole excitation by the $2p$ states) are calculated for all nuclei. These results are applied to new data for ^{192}Os. The sign of the quadrupole moment of the first excited 2^+ state is found to be negative; a previously reported measurement of its magnitude (−0.5 b) is inconsistent with the present experiment. Under the assumption that the transition charge is located near the nuclear surface, a new measurement of the quadrupole moment ($Q_{2^+} = -1.0$ b) is obtained. The equivalent quadrupole radius of the $0^+ \rightarrow 2^+$ transition is found to be 7.1 fm.

[NUCLEAR STRUCTURE Model-independent method for interpretation of dynamic hyperfine effect in muonic atoms. Measured muonic x-ray spectra ^{192}Os; deduced electric moments, charge parameters.]

I. INTRODUCTION

Since the beginning of muonic-atom physics, one of the central issues has been the extraction of nuclear sizes and shapes from experimental transition energies. For monopole charge radii, recent work has led to a so-called "model-independent" method of analysis[1,2] which depends upon the use of perturbation theory beginning from some reasonable trial charge distribution. Similar but more general methods also exist which treat both muonic-atom transition energies and elastic electron scattering cross sections within the same framework. A recent review of this subject may be found in Ref. 3.

For the extraction of information about nuclear deformations, no similar theory has been constructed. Here the situation is complicated in the most interesting cases by a strong quadrupole mixing of the muon $2p$ levels with the low-lying nuclear states (dynamic $E2$ effect). The result is a complex spectrum of many lines, which is customarily analyzed by means of a specific nuclear model. This model approach is conceptually similar to the early methods of analyzing monopole spectra.[4,5]

The purpose of the present work is twofold. First, we wish to show that the dynamic $E2$ effect may be analyzed by means of a "model-independent" method which is analogous to the monopole theory mentioned above. Second, we report new muonic-atom data for ^{192}Os and interpret it using this method. The paper is divided into six sections. In Sec. II, we summarize the calculational procedures by which a specific nuclear model may be compared with experimental measurements. In Sec. III, we discuss general modifications which may be made to these procedures to obtain "model-independent" analysis theories for both the monopole and multipole ($L > 0$) effects. In Sec. IV, we present the experimental methods and data for ^{192}Os. In Sec. V, we show how these data may be interpreted in terms of the analysis theories. In Sec. VI, the results are discussed and compared with other studies of ^{192}Os.

II. MODEL ANALYSIS

Given a specific nuclear model, it is in principle a straightforward procedure to compute the muonic energy levels. The Hamiltonian of the muon-nucleus system may be written as

$$H = H_N + H_\mu + H_{\rm int} + H' , \tag{1}$$

where H_N is the free nuclear Hamiltonian, H_μ is the muon Hamiltonian including the static spherically symmetric potential $V^{(0)}(r)$ which represents the average monopole electrostatic field generated by the nucleus, $H_{\rm int}$ is the residual muon-nuclear interaction [the difference between the true interaction $V(\vec{r})$ and the approximation $V^{(0)}(r)$], and H' includes all the otherwise neglected effects [e.g., quantum electrodynamics (QED)]. We denote the energy eigenvalues and eigenstates of H_N and H_μ by

$$H_N |\gamma IM\rangle = E_N^{(\gamma I)} |\gamma IM\rangle$$

and (2)

$$H_\mu |n\kappa m\rangle = E_\mu^{(n\kappa)} |n\kappa m\rangle ,$$

where IM are the spin and projection of the nuclear angular momentum, γ is an auxiliary nuclear quantum number, and $n\kappa m$ are the usual Dirac quantum numbers of the muon.

In the present work we assume that all effects included in H' are small and, therefore, may be treated in perturbation theory. These effects will be neglected in the discussions in the next two sections. In many instances $H_{\rm int}$ may also be treated as a perturbation, so that the energy eigenstates of the system are well represented by products of the eigenstates of H_N and H_μ. This possibility clearly depends upon making a good choice of $V^{(0)}(r)$; an optimum choice is

$$V^{(0)}(r) = \int \frac{d^3r'}{r_>} \langle \gamma IM | \rho(\vec{r}') | \gamma IM \rangle , \tag{3}$$

where $r_>$ is the greater of the nuclear and muon radial coordinates, and $\rho(\vec{r}')$ is the nuclear charge density operator. This choice is optimum in the sense that the first-order perturbed energy shift caused by $H_{\rm int}$ vanishes, except possibly for the effects of some higher multipoles in high-spin nuclei. The muon energy levels may now be found by solving the radial Dirac equations in the potential $V^{(0)}(r)$ and accounting for H' and $H_{\rm int}$ in first- or second-order perturbation theory.[6,7]

In some instances the off-diagonal matrix elements of $H_{\rm int}$ in the product basis $|\gamma IM\rangle |n\kappa m\rangle$ are large and comparable to the corresponding diagonal energy differences. This situation occurs particularly often for heavy deformed nuclei, where the muon $2p$ fine-structure splitting is of comparable magnitude to the collective, low-lying nuclear quadrupole excitations. The effects of this large interaction have been described in detail by Wilets,[8] Jacobsohn,[9] and Acker.[10] Although in these instances the treatment of $H_{\rm int}$ as a small perturbation is not appropriate, it is possible to make use of the solutions of H_N and H_μ by constructing a Hamiltonian matrix in the nearly degenerate subspace and diagonalizing it. The states of the system may be constructed by coupling nuclear states $|\gamma IM\rangle$ to muon states $|n\kappa m\rangle$ to give total angular momentum FM, denoted here by $|n\kappa\gamma I; FM\rangle$, or by the shorthand notation

$$|i\rangle \equiv |n_i \kappa_i \gamma_i I_i; F_i M_i\rangle . \tag{4}$$

For a longitudinal residual interaction expanded in multipoles L, the matrix elements of H are (Edmonds conventions[11])

$$\langle i | H | i' \rangle = [E_N^{(i)} + E_\mu^{(i)}]\delta_{ii'} - e^2(-1)^{I'+F+j'-j-1/2}\tfrac{1}{2}[1+(-1)^{l+l'+L}] \times \left[\frac{4\pi}{2L+1}(2j+1)(2j'+1)\right]^{1/2} \begin{Bmatrix} j' & I' & F \\ I & j & L \end{Bmatrix} \begin{pmatrix} j' & L & j \\ \frac{1}{2} & 0 & -\frac{1}{2} \end{pmatrix} W^{(ii')} , \tag{5}$$

where l and j are the muon orbital and total angular momenta and

$$W^{(ii')} = \int_0^\infty [F^{(i)}(r)F^{(i')}(r) + G^{(i)}(r)G^{(i')}(r)] \langle \gamma I \| \int d^3r' \rho(\vec{r}') Y_L(\hat{r}') r_<^L / r_>^{L+1} \| \gamma' I' \rangle dr . \tag{6}$$

The Hamiltonian in this basis breaks up into submatrices characterized by FM, which may each be diagonalized to yield the muon-nuclear energy levels. Truncation effects, as well as effects in H', may be treated in perturbation theory.[6]

III. ANALYSIS THEORIES

It is clear that fitting nuclear models to measured transition energies does not fully answer the basic empirical question of what the measurements imply about the nucleus. This question is addressed with some reservations by the "model-independent" analysis theories of the monopole distribution[1-3] which we summarize here in order to help develop the extension to the higher multipole case. The monopole theories generally begin with an approximate fit to the data with a trial charge distribution $\rho_0(r)$, which provides a set of trial energies $E_0^{(n\kappa)}$. Then if one considers arbitrary (but small) functional variations in $\rho_0(r)$, the change in a given muonic energy level due to this change in charge distribution is given to first order in perturbation theory as

$$E^{(n\kappa)} - E_0^{(n\kappa)} = -e^2 \int d^3r' [\rho(r') - \rho_0(r')] V_\mu^{(n\kappa)}(r') , \tag{7}$$

where

$$V_\mu^{(n\kappa)}(r') = \int_0^\infty \frac{dr}{r_>} [F^{(n\kappa)}(r)^2 + G^{(n\kappa)}(r)^2] \tag{8}$$

is the monopole electrostatic radial potential generated by the muon charge distribution, computed, e.g., from $\rho_0(r)$. Thus if one makes a reasonable guess about the trial nuclear charge distribution, Eq. (7) provides a useful integral constraint upon the true nuclear charge distribution $\rho(r')$. That is, if $E^{(n\kappa)}$ represents the measured muon energy, then the true nuclear charge distribution $\rho(r)$ must satisfy Eq. (7) to within the accuracy to which $E^{(n\kappa)}$ is known. A similar analysis may be carried through for elastic electron scattering cross sections. Instead of the muon-generated potentials $V_\mu(r')$, one obtains, in that case, other kernels which represent additional integral constraints.

For the analysis of muonic-atom data alone, a further approximation may be made. The kernel $V_\mu^{(n\kappa)}(r)$ [or $V_\mu^{(n\kappa)}(r) - V_\mu^{(n'\kappa')}(r)$ for a transition $n\kappa \rightarrow n'\kappa'$] may be approximated by the empirical form

$$V_\mu(r) = A + Br^k e^{-\alpha r} , \tag{9}$$

where values for the parameters A, B, k, and α, which depend upon the nucleus and the muon states under consideration, can be obtained from numerical fits to the computed muon potential. The constant term A contributes nothing to the energy shift in Eq. (7) since the variation of $\rho_0(r)$ is constrained by charge conservation. The energy shift thus becomes proportional to $\langle r^k e^{-\alpha r}\rangle - \langle r^k e^{-\alpha r}\rangle_0$. A model-independent radius parameter R_k can be defined by the relation

$$\frac{3}{R_k^3}\int_0^{R_k} r^{2+k} e^{-\alpha r} dr = \langle r^k e^{-\alpha r}\rangle , \tag{10}$$

so that R_k is the radius of a uniform charge distribution which has the expectation value $\langle r^k e^{-\alpha r}\rangle$. Equation (7) then reduces to

$$E^{(n\kappa)} - E_0^{(n\kappa)} = -Ze^2 B \frac{d\langle r^k e^{-\alpha r}\rangle}{dR_k}(R_k - R_k^{(0)}) . \tag{11}$$

Thus the measured muon energies $E^{(n\kappa)}$ can be represented by corresponding equivalent radii R_k, which provide a simple and concise summary of the measurements in terms of nuclear properties.

The muonic multipole analysis is slightly more complicated, but it may be developed in essentially the same way. In addition to the diagonal matrix elements of H, one can obtain from the experimental data the values of certain off-diagonal matrix elements as in Eq. (5). These matrix elements are not necessarily to be regarded as independently measured quantities as are the energies in the monopole case. Rather, they result from adjusting the Hamiltonian matrix to fit several observed eigenvalues simultaneously, and their determination may depend upon providing some physical constraints since the matrix may be underdetermined by the available experimental data. Such constraints can be obtained in various ways; one common method of providing them consists of using a specific nuclear model (e.g., the rotational model) to calculate relationships between the various matrix elements. The model parameters are then adjusted to best fit the observed data. A more general procedure which does not require the use of a particular nuclear model will be developed in the following paragraphs.

We assume for the moment that we have determined a set of matrix elements $\langle i|H|i'\rangle$ as in Eq. (5). The energy $E_\mu^{(i)}$ is to be interpreted as in the monopole case through Eq. (7) or Eq. (11). Apart from the nuclear energy $E_N^{(i)}$, which is presumed known from other experiments, we are left with the fitted quantities $W^{(ii')}$. These can be rewritten as

$$W^{(ii')} = \int d^3r' \rho_{ii'}(\vec{r}') V_\mu^{(ii')}(r') , \tag{12}$$

where

$$\rho_{ii'}(\vec{r}') = \langle \gamma I \| Y_L(\hat{r}')\, \rho(\vec{r}') \| \gamma' I' \rangle \tag{13}$$

is the reduced nuclear transition charge density, and where

$$V_\mu^{(ii')}(r') = \int_0^\infty dr [F^{(i)}(r)F^{(i')}(r) + G^{(i)}(r)G^{(i')}(r)] \frac{r_<^L}{r_>^{L+1}} \tag{14}$$

is the muon-generated radial transition potential. Thus the main physical result of such a fit is the determination of the values of certain weighted integrals over the nuclear transition charge densities. In analogy to Eq. (7), Eq. (12) provides a constraint which any candidate for the true transition charge density must satisfy. There is, however, an important difference between the monopole and multipole treatments. Equation (7) is valid only in perturbation theory, so that a reasonable initial guess for $\rho_0(r)$ is required. Equation (12) does not depend explicitly upon perturbation theory, so that no *a priori* knowledge of $\rho_{ii'}(\vec{r}')$ is required; rather, any candidate which satisfies Eq. (12) is acceptable.

The constraint represented by Eq. (12) may be parametrized in a way similar to that of the monopole case. We approximate the muon-generated transition potential by

$$V_\mu^{(ii')} \approx r^L (A + Br^m e^{-\alpha r}) \tag{15}$$

and determine the parameters A, B, m, and α as in the monopole case. In addition, we note that the reduced nuclear multipole matrix element is

$$M^{(ii')} = \int d^3r\, \rho_{ii'}(\vec{r}) r^L , \tag{16}$$

and can be related to the transition strength $B(EL)$ and static quadrupole moment Q_γ via the equations

$$B(EL;\gamma I \to \gamma' I') = \frac{e^2}{(2I+1)} \left| M^{(ii')} \right|^2 \tag{17}$$

and

$$Q_\gamma = \left(\frac{16\pi}{5}\right)^{1/2} \begin{pmatrix} I & 2 & I \\ -I & 0 & I \end{pmatrix} M^{(ii)}(L=2) . \tag{18}$$

Further, we can define an equivalent multipole radius R_m by means of

$$M^{(ii')} R_m^m e^{-\alpha R_m} = \int d^3r\, \rho_{ii'}(\vec{r}) r^{L+m} e^{-\alpha r} , \tag{19}$$

in which case

$$W^{(ii')} = M^{(ii')}(A + B R_m^m e^{-\alpha R_m}) . \tag{20}$$

R_m can be interpreted as the radius of a δ-function representation of $\rho_{ii'}$. The sensitivity of R_m with respect to variations in $W^{(ii')}$ for fixed $M^{(ii')}$ may be obtained by differentiating Eq. (20). As in the monopole analysis, this quantity is useful in assessing the significance of experimental uncertainties or model differences.

Often the magnitudes (and sometimes the signs) of $M^{(ii')}$ are known from other sources, such as Coulomb excitation measurements. In this case, Eq. (20) can be used to determine R_m. In any case Eq. (20) provides a concise way of specifying quantities actually determined by experiment. $M^{(ii')}$ here plays the role of normalization, as does the nuclear charge Z in the monopole case. However, in the multipole case normalization is known much less accurately and can introduce a significant uncertainty into the interpretation.

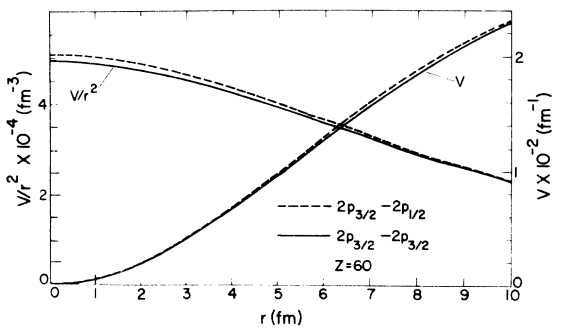

FIG. 1. Muon-generated quadrupole radial transition potentials for $Z=60$, defined by Eq. (14).

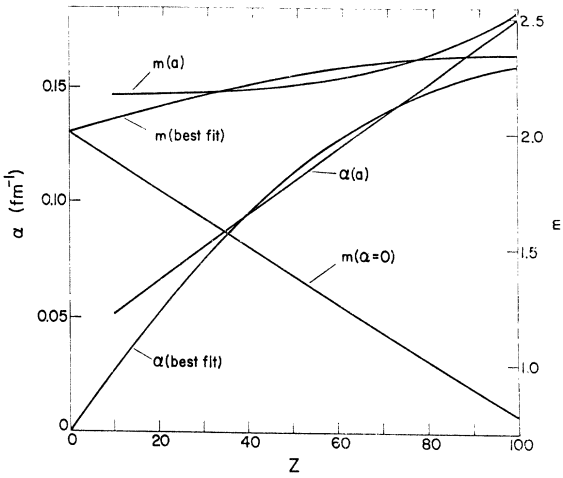

FIG. 2. Values of m and α fitted to the computed $2p_{3/2} - 2p_{3/2}$ quadrupole potential. Shown are the best fit values obtained by allowing both m and α to vary, as well as the values of m resulting from holding α fixed at zero and from using the α specified by the monopole formula of Ref. 13 [curves labeled (a)].

In a way which is similar to the combined muonic-atom elastic electron scattering analyses,[3] it is evident that the muonic multipole data may be combined with results of inelastic electron scattering experiments[12] to provide more information about transition charge densities. The multipole radius R_m is similar to the transition radius R_{tr} often dededuced from such scattering experiments, with the exception that different kernels are involved.

For numerical calculations, we now specialize to the most important case: the $L=2$ dynamic interaction involving the muon $2p$ states. The results presented here are obtained using the ground-state nuclear charge distribution

$$\rho(r) = \rho_0 \left[1 + \exp\left(\frac{r-c}{a}\right)\right]^{-1} \tag{21}$$

with $c = (1.183A^{1/3} - 0.414)$ fm and $a = 0.55$ fm, where A is the average mass for a given value of Z. The general appearance of the muonic kernels is illustrated in Fig. 1, where we have plotted the potential $V_\mu^{(ii')}$ for $Z=60$, both by itself and divided by r^2, for the $2p_{3/2} - 2p_{1/2}$ transition and the $2p_{3/2} - 2p_{3/2}$ diagonal cases. Because of the close similarity of these two curves, we have fitted only one of them, the $2p_{3/2}$-$2p_{3/2}$ potential, with the analytic form given in Eq. (15). The results of these fits, for values of Z covering the entire Periodic Table, are shown in Fig. 2. The curves labeled m(best fit) and α(best fit) result from a least-squares adjustment of all four parameters to fit the transition potential over the radial range where the nuclear charge is significant. The values of α are given to a very good approximation by the formula

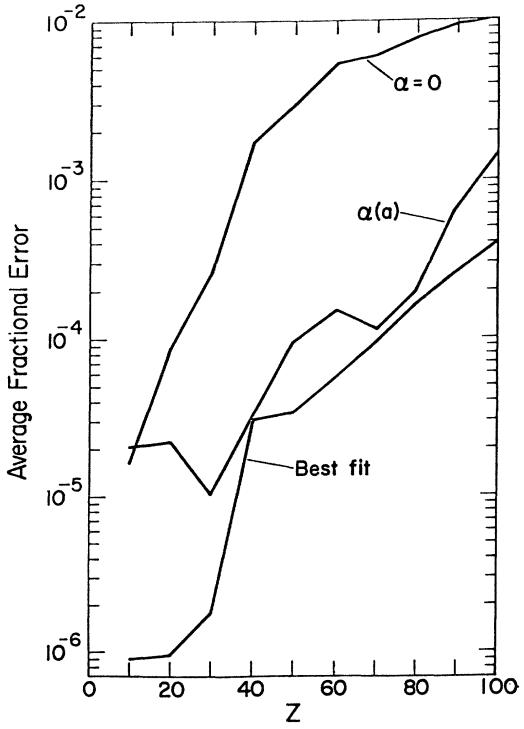

FIG. 3. Errors in the analytic approximations to the muon transition potentials. The values correspond to the choices of α shown in Fig. 2.

$$\alpha(\text{best fit}) \approx 0.00285Z - 0.0000126Z^2, \quad (22)$$

while

$$m(\text{best fit}) \approx 2 + 0.0065Z - 0.00003Z^2. \quad (23)$$

A good fit may also be obtained using values of α given by the formula of Engfer *et al.*[13] for monopole kernels. These values are indicated by the curve labeled $\alpha(a)$ in Fig. 2. The best values of m when α is fixed at $\alpha(a)$ are given by the curve $m(a)$. For yet a simpler representation, one may fix $\alpha = 0$; the appropriate values of m for this case are also shown in Fig. 2. The accuracy of these three fits is illustrated in Fig. 3, where we have plotted the fractional error, averaged over the nucleus, of the different approximations. As for the monopole kernels, the $\alpha = 0$ approximation is significantly less accurate. However, the inherently lower accuracy of the quadrupole information can make this approximation quite useful.

Values for the sensitivity of R_m to changes in $W^{(ii')}$ as expressed by the derivative $M^{(ii')}dR_m/dW^{(ii')}$ are shown in Fig. 4. These values are nearly independent of the choice of α, if m is chosen appropriately. The derivative is, however, sensitive to the choice of R_m, which here is taken to be equal to c in Eq. (21). The values in the figure may be altered using Eq. (20) to accommodate other choices of R_m.

It is possible to imagine two distinct systematic "model-independent" approaches in analyzing dynamic hyperfine spectra. One is to determine the parameters A, B, m, and α and use Eq. (20) to extract R_m directly, given known values of $M^{(ii')}$ and fitted values of $W^{(ii')}$. This procedure contains no direct reference to a nuclear transition charge density, and allows one to avoid computing muon wave functions and matrix elements as in Eq. (6). It should be noted, however, that the apparently strict model independence of this approach is somewhat compromised in two ways. The first is that some additional corrections are usually necessary (e.g., nuclear polarization and vacuum polarization), and these are somewhat model dependent. The second is that there is insufficient experimental information to determine the $2p_{3/2}$-$2p_{3/2}$ and the $2p_{3/2}$-$2p_{1/2}$ matrix elements independently; rather, they must be constrained in the fitting procedure and this constraint may introduce a slight model dependency. Nevertheless, this approach is useful and straightforward. To implement this approach, we have determined that the values of A and B are given (to within an accuracy of better than 2% for $Z > 50$) by the formulas:

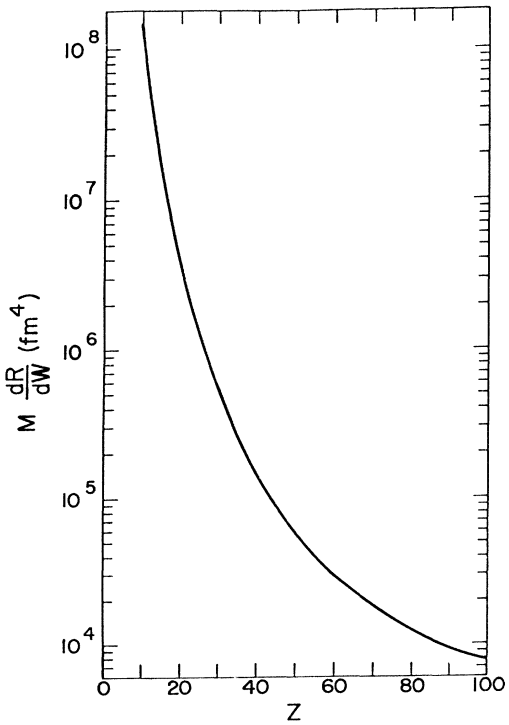

FIG. 4. Values of the derivative of Eq. (20) in the text, evaluated for $R = 1.183A^{1/3} - 0.414$, where A is the average atomic mass for each Z.

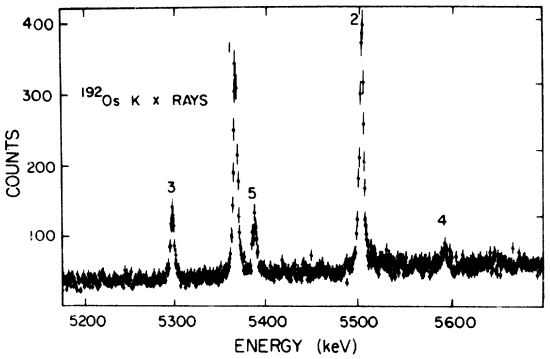

FIG. 5. Spectrum of muonic $2p$-$1s$ transitions observed for ^{192}Os. The peak numbers correspond to the transitions listed in Table I and Fig. 7.

$$A \approx -3.0657 \times 10^{-5} + 9.0899 \times 10^{-10} \times (Z^{3.5033} e^{-0.01797Z})\ \text{fm}^{-3} \quad (24)$$

and

$$B \approx 1.1752 \times 10^{-6} - 7.7990 \times 10^{-12} \times (Z^{3.4458} e^{-0.00908Z})\ \text{fm}^{-(3+m)}. \quad (25)$$

The corresponding values of m and α are given by Eqs. (22) and (23). It is this approach which is developed in Sec. V for ^{192}Os.

One may also follow a second approach which is closer to that usually used in the monopole case. This involves using a specific nuclear model for the transition charge densities, and fitting the experimental data in the usual way, i.e., by adjusting the appropriate nuclear model parameters. Then the model-independent parameter R_m may be extracted from the fitted charge density by use of Eqs. (16) and (19). This approach has the advantage of having fewer fitted parameters, since only m and α must be known (even the derivative $M\,dR/dW$ may be calculated for the problem at hand by making small variations in the transition charge density).

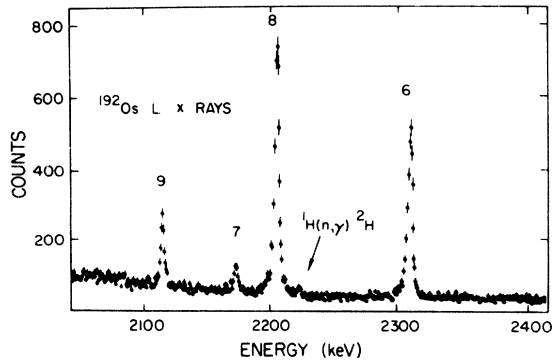

FIG. 6. Spectrum of muonic $3d$-$2p$ transitions observed for ^{192}Os. The peak numbers correspond to the transitions listed in Table I and Fig. 7.

Both methods for obtaining R_m are in principle equivalent; which is more appropriate in a particular case depends upon the point of view and the resources at hand.

IV. EXPERIMENTAL RESULTS

The muonic x-ray spectrum of an isotopically separated target[14] of ^{192}Os was obtained at LAMPF during an initial period of low intensity accelerator operation. The experimental arrangement and the data analysis techniques were essentially the same as those of Ref. 7. The primary difference between this experiment and that reported in Ref. 7 resulted from the higher x-ray energies of muonic ^{192}Os as compared with the x-ray energies reported in that work. In particular, calibration of the ^{192}Os muonic x-ray energies was derived from a simultaneously accumulated spectrum of an isotopically separated ^{208}Pb target. The energies of the ^{208}Pb x-ray spectrum were taken from Ref. 15. Corrections were included for geometrical effects and detector system nonlinearity.[7,16] Portions of the spectral data which are relevant to the present discussion are shown in Figs. 5 and 6. In these figures the lines are numbered to correspond with Table I which lists the measured line energies and relative intensities.

V. ANALYSIS

We proceed to interpret the observed muonic hyperfine structure of ^{192}Os using the methods discussed in Sec. III. In this discussion we will con-

TABLE I. Experimentally measured K and L transition energies and relative intensities of ^{192}Os. The statistical errors listed were used to determine the uncertainties of the hyperfine splittings and do not include errors due to uncertainties in the calibration energies of ^{208}Pb. This calibration error is about 400 eV for the K transitions and about 100 eV for the L transitions. These errors should be added to the listed statistical errors to obtain absolute errors. The relative intensities for each group of transitions (K and L) were normalized to 100%.

Transition	Index	Experiment energy (keV)	Statistical error (keV)	Relative intensity (%)
$2p$-$1s$	4	5592.67	0.59	2.9
	2	5502.76	0.10	41.8
	5	5387.49	0.20	9.3
	1	5366.55	0.09	35.1
	3	5297.00	0.17	10.9
$3d$-$2p$	6	2309.19	0.07	35.9
	8	2204.96	0.06	47.2
	7	2173.08	0.18	4.7
	9	2114.51	0.08	12.2

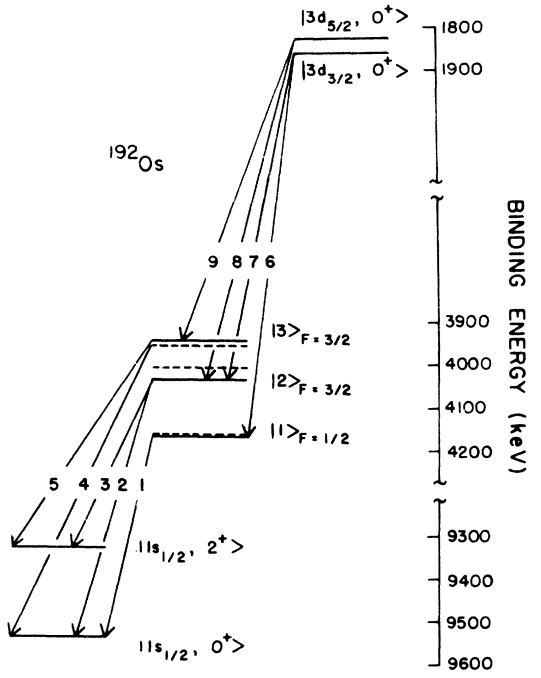

FIG. 7. Energy level diagram of muonic ^{192}Os. The highly mixed $2p$ state wave functions were calculated to be

$$|1\rangle_{F=1/2} = -0.9904|2p_{1/2}, 0_1^+\rangle + 0.1374|2p_{3/2}, 2_1^+\rangle + 0.0173|2p_{3/2}, 2_2^+\rangle,$$

$$|2\rangle_{F=3/2} = 0.8762|2p_{3/2}, 0_1^+\rangle + 0.4480|2p_{1/2}, 2_1^+\rangle, -0.1773|2p_{3/2}, 2_1^+\rangle + 0.0130|2p_{1/2}, 2_2^+\rangle - 0.0054|2p_{3/2}, 2_2^+\rangle,$$

$$|3\rangle_{F=3/2} = 0.4627|2p_{3/2}, 0_1^+\rangle - 0.8818|2p_{1/2}, 2_1^+\rangle + 0.0582|2p_{3/2}, 2_1^+\rangle + 0.0220|2p_{1/2}, 2_2^+\rangle - 0.0673|2p_{3/2}, 2_2^+\rangle.$$

The dashed lines represent the unperturbed positions of the $|2p_{1/2}, 0_1^+\rangle$, $|2p_{3/2}, 0_1^+\rangle$, and $|2p_{1/2}, 2_1^+\rangle$ levels.

sider only the dynamic hyperfine effect in the $2p$ states. A separate analysis performed as part of this work indicated that the dynamic hyperfine interaction in the $3d$ and higher muonic states is quite small (<300 eV in the $3d$ states). These effects, although small, were included in the final analysis. An energy level diagram of the observed muonic states is shown in Fig. 7. In the figure, the dynamically mixed $2p$ levels are shown along with the positions (indicated by dashed lines) at which the levels would occur in the absence of the dynamic interaction.

To obtain approximate nuclear charge parameters for ^{192}Os so that, for example, the "unperturbed" binding energies of the $2p_{1/2}$ and $2p_{3/2}$ muonic states can be computed, it was convenient to assume a specific form for the nuclear charge distribution and adjust the parameters of that distribution until the $1s_{1/2}$ muonic binding energy was reproduced. For this adjustment the K and L transitions which involve the $|2p_{1/2}, 0^+; F=\frac{1}{2}\rangle$ state (lines 1 and 6 in Fig. 7) were used since this state is the $2p$ state least affected by the dynamic quadrupole interaction. A three-parameter Fermi distribution [Ref. 17, Eq. (8)] was used to represent the nuclear charge distribution. In this model β was fixed at 0.17, a reasonable value in terms of the measured $B(E2; 0^+ \rightarrow 2_1^+)$.[18-20] The parameters c and t were adjusted to fit the observed energies of transitions 1 and 6. In this adjustment, corrections were included for quantum electrodynamic, nuclear polarization, electron screening, and relativistic effects.[5] Such a procedure allows an approximate representation for the monopole part of the nuclear charge distribution to be extracted from the observed spectra in spite of the presence of the large dynamic quadrupole interaction.

The second step in the analysis was an iterative process in which the coefficients $W^{(ii')}$ of Eq. (5) were varied to fit the hyperfine splitting of the $2p$ states as obtained from the observed $3d$-$2p$ and $2p$-$1s$ transitions. This involved making an initial guess of the values of the coefficients [guided by measured quadrupole moments or $B(E2)$ values and employing Eqs. (17), (18), and (20)[21]] followed by a diagonalization of the Hamiltonian matrix of Eq. (5). This diagonalization yields mixed wave functions which are then used in a cascade calculation to compute the expected x-ray intensities and energies for that set of $W^{(ii')}$. The procedure follows the calculational techniques discussed in Ref. 5, except that matrix elements are varied independently rather than being calculated from a specific nuclear model.

When an approximate fit to the $2p$ hyperfine structure was obtained, the monopole charge parameters c and t were slightly adjusted to correct for the small quadrupole perturbation of lines 1 and 6. The procedure was iterated until a best fit to the entire experimental spectrum was obtained.

Table II summarizes our results for the monopole part of the nuclear charge distribution of ^{192}Os. Also given in Table II are the calculated energies of the "equivalent" muonic transitions in the absence of the dynamic quadrupole interaction, the parameters used to fit the muon-generated radial potential, and the sensitivity C_Z.

In ^{192}Os the dynamic quadrupole interaction is dominated by the first excited nuclear state ($I^\pi = 2^+$, $E = 205.8$ keV). The second excited state ($I^\pi = 2^+$, $E = 489.1$ keV) was included in the calculations but because the excitation energy of this level is far removed from the unperturbed $2p$ fine-structure splitting energy (≈153 keV), the influence of this

TABLE II. Parameters derived from the monopole part of the nuclear charge distribution of ^{192}Os. The "equivalent" transition energies listed were calculated from the monopole part of the charge distribution in the absence of the dynamic $E2$ interaction (see text). The errors given for E and R_K (listed in parentheses) represent only the experimental errors and do not include theoretical uncertainties, i.e., those due to nuclear polarization. The parameter α was obtained from the prescription given in Ref. 13.

Equivalent transition	Equivalent energy E	K	α (fm^{-1})	C_Z (fm/keV)	R_K (fm)
$2p_{1/2}$-$1s_{1/2}$	5373.49(50)	2.2929	0.1445	-1.650×10^{-3}	6.9198(8)
$2p_{3/2}$-$1s_{1/2}$	5526.85(50)	2.3073	0.1445	-1.582×10^{-3}	6.9209(8)
$3d_{3/2}$-$2p_{1/2}$	2302.51(20)	3.6172	0.1445	-1.235×10^{-2}	7.011(2)
$3d_{3/2}$-$2p_{3/2}$	2149.16(20)	4.0206	0.1445	-1.822×10^{-2}	7.037(4)
$3d_{5/2}$-$2p_{3/2}$	2180.98(20)	4.0206	0.1445	-1.803×10^{-2}	7.037(4)

state on the observed spectrum is small. Hence, it was not possible to determine from our data the $W^{(ii')}$ which involve this state. Nevertheless, the state does have a slight influence[22] and its effects must be included in the calculations, at least approximately. We estimated the relevant $W^{(ii')}$ for this state (see Table III) from measured $B(E2)$ values[18-20] and the theoretical quadrupole moment[23] via Eqs. (17), (18), and (20).

In order to limit the number of fitted $W^{(ii')}$ to two, use was made of the similarity of the $(2p_{1/2}$-$2p_{3/2})$ and $(2p_{3/2}$-$2p_{3/2})$ muon kernels as illustrated in Fig. 1. According to calculations using various model charge densities, the difference in the $W^{(ii')}$ which involve the two kernels is less than 1.0%. Furthermore, this difference is insensitive to the choice of nuclear charge model used in the calculations.[24] In the present calculations using a three-parameter Fermi model the $(2p_{1/2}$-$2p_{3/2})$ kernel is larger by 0.4%. We have constrained the $W^{(ii')}$ using this numerical value.

The values of the $W^{(ii')}$ and R_m derived from the ^{192}Os data are given in Table IV. The error values given in parentheses result from the following considerations. First, there is experimental error due to uncertainty in the determination of the hyperfine structure. This error contribution was derived from the least-squares fitting routine used to determine the fitted $W^{(ii')}$ and took into account the correlation between the fitted elements. Second, there is error due to uncertainty in the $W^{(ii')}$ which involves the second excited nuclear state. This error was estimated by individually varying the $W^{(ii')}$ involving this state by 10% and refitting the data. The final error is due to nuclear polarization and is perhaps the largest source of uncertainty in the present work. This error arises from two considerations. First, nuclear polarization corrections cause the measured matrix elements to be renormalized by a few percent.[6] We have chosen this renormalization factor to be 1.04 $\pm$0.03, in agreement with values given in Ref. 6. Second, because the nuclear polarization correction in the $1s_{1/2}$ muon state has a significant uncertainty, there exists an uncertainty in the determination of the monopole nuclear charge distribution and consequently a slight uncertainty in the $2p$ fine structure splitting which is computed using this charge distribution. The uncertainty in

TABLE III. The $W^{(ii')}$ and $M^{(ii')}$ relevant to the second excited state in ^{192}Os (see text). The $M^{(ii')}$ were taken from Refs. 18–20 and 23.

$I\rightarrow I'$	$W^{(ii')}$ ($\times10^{-2}$ fm^{-1})	$M^{(ii')}$ ($\times10^{2}$ fm^{2})
$0^+\rightarrow 2_2^+$	2.25	0.45(1)
$2_1^+\rightarrow 2_2^+$	6.75	1.34(6)
$2_2^+\rightarrow 2_2^+$	2.26	0.45

TABLE IV. The $W^{(ii')}$, $M^{(ii')}$, and R_m for ^{192}Os. Only the $W^{(ii')}$ involving the $(2p_{3/2}$-$2p_{3/2})$ muon kernel are given. Those involving the $(2p_{1/2}$-$2p_{3/2})$ kernel are 1.004 times larger. The $M^{(ii')}$ were obtained from the Coulomb excitation data of Refs. 18–20 and 25. The equivalent quadrupole charge radii R_m are given for the transitional $0^+\rightarrow 2_1^+$ and static $2_1^+\rightarrow 2_1^+$ nuclear charge densities. Only an upper limit is placed on the static R_m since the value given for $M^{(ii)}$ is not compatible with the measured $W^{(ii)}$ in this case (see text). The parameters of Eq. (15) used to represent the muon-generated quadrupole radial potential were the "best fit" values discussed in Sec. III. The sensitivity of R_m is $M^{(ii')}dR_m/dW^{(ii')} = -1.5\times10^{4}$ fm^4.

$I\rightarrow I'$	$W^{(ii')}$ ($\times10^{-2}$ fm^{-1})	$M^{(ii')}$ (from Coul. excit.) ($\times10^{2}$ fm^{2})	R_m (fm)
$0^+\rightarrow 2_1^+$	7.07(21)	1.43(2)	7.27(22)
$2_1^+\rightarrow 2_1^+$	−6.55(58)	−0.66(26)	$\leq$5.8(?)

the $2p$ fine structure splitting due to the uncertainty in the nuclear polarization was estimated to be 400 eV. The $W^{(ii')}$ were refitted using this change in the $2p$ fine structure in order to determine the uncertainty introduced by the effect. The final error quoted in Table IV is a quadratic sum of all the sources of error discussed above.

VI. DISCUSSION

It is evident from Eq. (5) that the calculated hyperfine structure depends upon the relative phases of the $W^{(ii')}$ for the various states. The phase dependence is similar to that encountered in the analysis of Coulomb excitation experiments.[25] However, in the case of the muonic dynamic hyperfine interaction, information can be derived not only from the observed hyperfine energy separations but also from the relative intensities of the various hyperfine components. When the experimental data are of good quality, this additional information can be used to decide among the various possible relative phases.

In the nuclear reorientation measurements of Ref. 26 two phase combinations[27] gave equally satisfactory fits to the ^{192}Os data and therefore a unique determination of the sign of Q_{2^+} was not possible. We found, when analyzing the muonic x-ray data, that hyperfine structure computations which used the phase combinations that correspond to a negative quadrupole moment for the first excited 2^+ state gave significantly better agreement with the observed hyperfine transition intensities than did those with a positive quadrupole moment (χ^2/degree of freedom = 1.1 and 9.5 in the two cases). Therefore, we are able to determine that the sign of the quadrupole moment of the first 2^+ state of ^{192}Os is negative.

In comparing the values of R_m and R_K, it is clear that the $0^+ \rightarrow 2^+$ transition quadrupole charge density is concentrated near the nuclear surface. This observation is consistent with electron scattering results from spherical nuclei[12] and with results of muonic x-ray studies of strongly deformed rotational nuclei such as tungsten.[17]

Similarly, a value of R_m can, in principle, be computed for the static $(2^+ \rightarrow 2^+)$ quadrupole charge density of the 2^+ state by combining the $W^{(ii')}$ measured in this work with the value of $M^{(ii')}$ for this state derived from Refs. 25 and 26. However, when this procedure is attempted, no physical solution for R_m can be obtained, indicating that the value of Q_{2^+} reported in Refs. 25 and 26 (−0.5 b) is inconsistent with the $W^{(ii')}$ measured in the present work. With presently available data, we are therefore unable to derive a value of R_m for the 2^+ state of ^{192}Os.

However, if we assume, following the prediction of the rotational model, that R_m for the 2^+ state is equal to the value of R_m obtained for the $0^+ \rightarrow 2^+$ transition charge density, it is possible to derive a value for $M^{(ii')}$ and consequently a quadrupole moment for the 2^+ state from our data. With this assumption we obtain a value $Q_{2^+} = -1.0$ b. We note that this value lies between the rotational model prediction (−1.3 b) and the prediction of the triaxial model[28] (−0.8 b) but is not in agreement with the prediction of Kumar and Baranger[29] (−0.36 b).

In order to resolve the discrepancy noted above and to exploit the full power of the proposed method of quadrupole analysis to provide insight into the radial distribution of the quadrupole charge density, it is clear that a remeasurement of Q_{2^+} is desirable.

Note added in proof. A recent Coulomb excitation measurement [P. Russo, D. Cline and J. Sprinkle, Bull. Am. Phys. Soc. 22, 545 (1977) and P. Russo, private communication] gives for ^{192}Os a value $Q_{2^+} = -0.81(15)$ b. Combining this value with the $W^{(ii')}$ measured in the present work yields $R_m = 5.6^{+2.1}_{-3.1}$ fm for the static quadrupole charge density of the 2^+ state. Although the uncertainty is large, this value is reasonably consistent with the value observed for the $0^+ \rightarrow 2^+$ transition charge density.

ACKNOWLEDGMENTS

The authors wish to thank R. M. Steffen for helpful discussions concerning this work. We are also indebted to M. V. Hoehn for a critical reading of the manuscript.

---

†Work supported by the U. S. Energy Research and Development Administration and the Institute für Kernphysik, KFA Jülich, Germany.

*Present address: Department of Physics, Xavier University, Cincinnati, Ohio 45207.

[1]K. W. Ford and J. G. Wills, Phys. Rev. 185, 1429 (1969).

[2]R. C. Barrett, Phys. Lett. 33B, 388 (1970).

[3]J. L. Friar and J. W. Negele, Advan. Nucl. Phys. 8, 219 (1975).

[4]H. L. Acker, J. Marshall, G. Backenstoss, and D. Quitman, Nucl. Phys. 62, 477 (1965).

[5]S. Devons and I. Duerdoth, Advan. Nucl. Phys. 2, 295 (1969).

[6]M. Y. Chen, Phys. Rev. C 1, 1167, 1176 (1970).

[7]E. B. Shera, E. T. Ritter, R. B. Perkins, G. A. Rinker, L. K. Wagner, H. D. Wohlfahrt, G. Fricke, and R. M. Steffen, Phys. Rev. C 14, 731 (1976).

[8]L. Wilets, K. Dan. Vidensk. Selsk. Mat.-Fys. Medd. 29, No. 3 (1954).

[9]B. A. Jacobsohn, Phys. Rev. 96, 1637 (1954).
[10]H. L. Acker, Nucl. Phys. 87, 153 (1966).
[11]A. R. Edmonds, *Angular Momentum in Quantum Mechanics* (Princeton U.P., Princeton, N.J., 1957).
[12]R. Neuhausen, in Proceedings of the Saclay Meeting on Electron Scattering at Medium Energy, September 1975 (unpublished).
[13]R. Engfer, H. Schneuwly, J. L. Vuilleumier, H. K. Walter, and A. Zehnder, At. Data Nucl. Data Tables 14, 509 (1974).
[14]The 79-g target of ^{192}Os was obtained on loan from the ERDA Research Pool and had an isotopic purity of 99.06%.
[15]D. Kessler, H. Mes, A. C. Thompson, H. L. Anderson; M. S. Dixit, C. K. Hargrove, and R. J. McKee, Phys. Rev. C 11, 1719 (1975).
[16]E. B. Shera, Phys. Rev. C 12, 1003 (1975).
[17]D. Hitlin, S. Bernow, S. Devons, I. Duerdoth, J. W. Kast, E. R. Macagno, J. Rainwater, C. S. Wu, and R. C. Barrett, Phys. Rev. C 1, 1184 (1970).
[18]W. T. Milner, F. K. McGowan, R. L. Robinson, P. H. Stelson, and R. O. Sayer, Nucl. Phys. A177, 1 (1971).
[19]R. F. Casten, J. S. Greenberg, S. H. Sie, G. A. Burginyon, and D. A. Bromley, Phys. Rev. 187, 1532 (1969).
[20]F. K. McGowan and P. H. Stelson, Phys. Rev. 122, 1274 (1961).
[21]To employ Eq. (20), a reasonable value of R_m must be assumed. A good initial assumption is to let the quadrupole charge density be concentrated at the surface of the nucleus and to set $R_m \approx R_K$.
[22]M. Ikeda, A. Ikeda, and R. K. Sheline, Phys. Lett. 45B, 187 (1973).
[23]K. Kumar, Phys. Lett. 29B, 25 (1969).
[24]This fact has been pointed out in previous works such as H. L. Acker, Nucl. Phys. 87, 153 (1966).
[25]S. A. Lane and J. X. Saladin, Phys. Rev. C 6, 613 (1972).
[26]R. J. Pryor and J. X. Saladin, Phys. Rev. C 1, 1573 (1970).
[27]Although it was not explicitly stated in Ref. 26, we note that of the four possible phase combinations of P_4 and Q_{2^+} (in the notation of Ref. 23), only two are consistent with the results of Ref. 26; namely those in which P_4 and Q_{2^+} have the same (not opposite) signs.
[28]A. S. Davydov and G. F. Filippov, Nucl. Phys. 8, 237 (1958).
[29]K. Kumar and M. Baranger, Nucl. Phys. A122, 273 (1968).